Article

Discovery Medicine 2025; 37(202): 2624–2636
https://doi.org/10.24976/Discov.Med.202537202.220

AURKA Knockdown Induces Apoptosis in Human Lung Cancer Cell Lines A549 and H1299 by Regulating Mitochondrial Function and Reactive Oxygen Species

Xinde Wang[1], Lijun Xie[2,*]

[1]Department of Respiratory and Critical Care Medicine, Taishun County People's Hospital, 325500 Wenzhou, Zhejiang, China
[2]Department of Respiratory and Critical Care Medicine, The Third People's Hospital of Cangnan County, 325804 Wenzhou, Zhejiang, China
*Correspondence: 13858756817@163.com (Lijun Xie)
Submitted: 29 July 2025 Revised: 2 September 2025 Accepted: 17 September 2025 Published: 20 November 2025

Background: Aurora kinase A (AURKA) has been reported to play an oncogenic role in non-small cell lung cancer (NSCLC). However, its specific role in regulating mitochondrial function and reactive oxygen species (ROS) in NSCLC cells remains unclear. This study aimed to investigate the function of AURKA in NSCLC, with a particular focus on its regulation of mitochondrial activity and ROS levels in A549 and H1299 cell lines.

Methods: AURKA expression and protein localization in lung adenocarcinoma (LUAD) were analyzed using publicly available gene expression and immunohistochemistry datasets. Small interfering RNA (siRNA) was used to knock down AURKA expression in A549 and H1299 cell lines. To evaluate cellular proliferation, migration, and invasion capabilities, a series of assays were performed, including cell counting kit-8 (CCK-8), colony formation, 5-ethynyl-2′-deoxyuridine (EdU) incorporation, Transwell migration/invasion, and wound healing assays. Mitochondrial function was assessed by measuring mitochondrial membrane potential, nicotinamide adenine dinucleotide/reduced nicotinamide adenine dinucleotide (NAD^+/NADH) ratio, adenosine triphosphate (ATP) levels, and ROS generation. Apoptosis was evaluated using terminal deoxynucleotidyl transferase dUTP nick end labeling staining, western blot analysis, and caspase activity assays. N-acetylcysteine (NAC) was used in rescue experiments to further investigate the role of oxidative stress.

Results: AURKA was significantly upregulated in LUAD tissues with higher protein expression confirmed by immunohistochemistry data, correlating with poor prognosis ($p < 0.05$). Targeted inhibition of AURKA expression resulted in diminished proliferative, migratory, and invasive behaviors in NSCLC cells ($p < 0.05$). AURKA silencing induced mitochondrial dysfunction, decreased NAD^+/NADH ratio and ATP production, and increased ROS levels, resulting in enhanced apoptosis ($p < 0.05$). NAC treatment partially reversed these effects ($p < 0.05$).

Conclusion: AURKA maintains mitochondrial integrity and redox homeostasis in NSCLC cells, thereby suppressing ROS-mediated apoptosis. Targeting AURKA and oxidative stress pathways may represent a promising therapeutic strategy for NSCLC.

Keywords: AURKA; non-small cell lung cancer; mitochondrial dysfunction; oxidative stress; apoptosis

Introduction

Lung cancer is one of the most frequently diagnosed malignancies worldwide, ranking second in incidence and remaining the leading cause of cancer-related mortality, thus representing a major global health concern. In 2020 alone, approximately 220,000 new cases and 179,000 deaths were attributed to lung cancer worldwide [1].

Histopathologically, lung cancer is broadly classified into two main types: small-cell lung cancer (SCLC) and non-small cell lung cancer (NSCLC). NSCLC is further subdivided into lung adenocarcinoma (LUAD), squamous cell carcinoma, large cell carcinoma, and other less common subtypes, with LUAD being the most prevalent, accounting for approximately 40% of cases [2,3]. Despite advances in surgery, radiotherapy, and chemotherapy [4], patients with advanced or metastatic NSCLC—including LUAD—continue to have limited therapeutic options and poor clinical outcomes. These challenges underscore the urgent need for more effective treatment strategies. In response, this study aimed to elucidate the molecular mechanisms underlying LUAD progression and to explore novel avenues for its prevention and therapeutic intervention.

Aurora kinase A (AURKA), a serine/threonine kinase by classification, functions as a well-established oncogene and is highly expressed in actively proliferating cells. Its overexpression has been linked to several malignant cellular processes, including genomic instability, aneuploidy, and aberrant centrosome duplication [5]. Elevated AURKA

expression has been widely reported across various cancers, including ovarian, prostate, and head and neck tumors, where it is frequently associated with poor prognosis and unfavorable clinical outcomes [6].

Within colorectal cancer models, suppression of AURKA activity in cells lacking ARID1A has been demonstrated to induce a halt in cell cycle progression specifically at the G2/M checkpoint, along with promoting programmed cell death, thereby underscoring its value as a potential therapeutic approach for molecularly stratified tumor subgroups [7]. In lung cancer, particularly NSCLC, the Aurora kinase family—represented by AURKA and AURKB—has been strongly implicated in tumorigenesis and disease progression. Elevated expression of these kinases is associated with poor clinical prognosis and is linked to increased cellular motility, invasiveness, and resistance to both chemotherapy and radiotherapy [8]. Notably, knockdown of AURKA has been shown to suppress tumor growth in both *in vitro* and *in vivo* models. Furthermore, AURKA, along with its downstream effector C-X-C motif chemokine ligand 5, has been found to promote radioresistance by inducing cytotoxic autophagy in NSCLC cells [9]. Collectively, these findings underscore AURKA as a critical driver of cancer progression and therapeutic resistance, suggesting that its targeted inhibition may offer a promising strategy to induce apoptosis and improve treatment outcomes in lung adenocarcinoma. Apoptosis regulated by mitochondrial pathways is crucial for cancer cell fate, where mitochondrial impairment and elevated reactive oxygen species (ROS) levels act as major inducers of intrinsic apoptotic mechanisms [10]. Increasing evidence suggests that AURKA participates in maintaining mitochondrial stability and modulating oxidative stress responses [11].

Based on these findings, this investigation focuses on elucidating how AURKA inhibition triggers apoptosis in lung adenocarcinoma cells, with a particular focus on its regulation of mitochondrial function and ROS generation. This study is expected to yield valuable insights into the clinical relevance of AURKA inhibition as a potential treatment strategy for lung adenocarcinoma.

Materials and Methods

Bioinformatic Analysis

The expression and prognostic significance of AURKA in LUAD were investigated through a combination of online database analysis. Stage-specific expression patterns of AURKA and overall survival (OS) analysis were assessed using GEPIA2 (http://gepia2.cancer-pku.cn/). The "Stage Plot" module was used to evaluate expression across cancer stages, while the "Survival" module was used to generate OS curves, with log-rank *p* values indicating statistical significance.

Immunohistochemical (IHC) staining data of lung adenocarcinoma and corresponding normal lung tissues were obtained from the Human Protein Atlas (HPA, https://www.proteinatlas.org/) to evaluate AURKA protein expression patterns. Staining intensity and distribution were compared between tumor and normal samples.

Cell Culture and Cell Transfection

Cell lines A549 (#CL-0016), H1299 (#CL-0165), PC-9 (#CL-0668), and H1975 (#CL-0298) were obtained from Procell (Wuhan, China) and cultured in RPMI-1640 medium (#11875-093, GIBCO BRL, Grand Island, NY, USA) supplemented with 10% fetal bovine serum (FBS; #10099-141, GIBCO BRL), 100 U/mL penicillin, and 100 µg/mL streptomycin (#15140-122, GIBCO BRL). BEAS-2B cells (#SNL-203, SUNNCELL, Wuhan, China) were maintained in Bronchial Epithelial Cell Growth Medium (#CC-3170, Lonza, Walkersville, MD, USA). All cells were incubated at 37 °C with 5% CO_2 in a humidified atmosphere. Twenty-four hours prior to transfection, cells were seeded into six-well plates at a density of 2×10^5 cells per well to achieve approximately 70% confluence. All cell lines were authenticated by short tandem repeat (STR) profiling and regularly confirmed to be mycoplasma-free.

AURKA-specific small interfering RNAs (siRNAs) and corresponding negative control siRNAs (si-NC) were synthesized by GenePharma Co., Ltd. (Shanghai, China). The siRNA sequences used in this study are listed in Table 1.

Cellular transfection was performed utilizing the Lipofectamine™ 2000 reagent (#11668019; Thermo Fisher Scientific, Waltham, MA, USA) following the manufacturer's instructions. After a 6-hour incubation with the transfection mixture, the cells were replenished with fresh, complete culture medium. Subsequent experiments were initiated 48 hours after the completion of the transfection protocol.

Table 1. siRNA sequences.

siRNA type	Sequence
si-AURKA	Sense: 5′-AUGCCCUGUCUUACUGUCATT-3′
	Antisense: 5′-UGACAGUAAGACAGGGCAUTT-3′
si-NC	Sense: 5′-UUCUCCGAACGUGUCACGUTT-3′
	Antisense: 5′-ACGUGACACGUUCGGAGAATT-3′

siRNA, small interfering RNA; AURKA, Aurora kinase A; si-NC, negative control siRNAs.

Cell Counting Kit-8 (CCK-8) Assay

Cellular proliferation was assessed using the cell counting kit-8 (CCK-8; #96992, Sigma-Aldrich, St. Louis, MO, USA) according to the manufacturer's instructions. A549 and H1299 cells were seeded into 96-well plates at a density of 3×10^3 cells per well and incubated for 0, 12, 24, and 48 hours. At each time point, 10 µL of CCK-8 so-

lution was added to each well, followed by incubation at 37 °C for 60 minutes. Absorbance was then measured at 450 nm using a microplate reader (iMark™, Bio-Rad, Hercules, CA, USA).

Colony Formation

To evaluate clonogenic potential, A549 and H1299 cells were seeded at a low density of 500 cells per well in standard 6-well culture plates. The cells were then maintained under appropriate growth conditions for a continuous period of 14 days, allowing sufficient time for visible colony formation to occur.

After incubation, colonies were fixed with 4% paraformaldehyde (#P1110, Solarbio, Beijing, China) for 15 minutes and then stained with 0.1% crystal violet (#C0121, Beyotime, Shanghai, China) for 20 minutes. The wells were gently washed with phosphate-buffered saline (PBS) and air-dried. Colonies containing more than 50 individual cells were manually counted to assess clonogenic growth under an inverted light microscope (Olympus CKX53, Olympus, Tokyo, Japan).

EdU Assay

Cell proliferation was assessed using the 5-ethynyl-2′-deoxyuridine (EdU) incorporation assay with Alexa Fluor 647 labeling (#C0075L, Beyotime, Shanghai, China), following the manufacturer's protocol. A549 and H1299 cells were seeded into 24-well plates at 5×10^4 cells per well and incubated overnight for adherence. The cells were then incubated with 10 μM EdU at 37 °C for 2 hours. Subsequently, cells were fixed with 4% paraformaldehyde (#P1110, Solarbio, Beijing, China) for 30 minutes at room temperature, followed by permeabilization with 0.3% Triton X-100 for 15 minutes.

The Click-iT reaction mixture containing Alexa Fluor 647 azide was added and incubated in darkness for 30 minutes. Subsequently, cell nuclei underwent counterstaining with 4',6-diamidino-2-phenylindole (DAPI) at a concentration of 1 μg/mL (#C1002, Beyotime, Shanghai, China) for 10 minutes at ambient temperature. Fluorescence microscopy images were captured utilizing an Olympus IX73 microscope (Olympus, Tokyo, Japan). Quantification of EdU-positive cells, indicated by red fluorescence, along with total nuclei stained blue, was performed in five randomly chosen microscopic fields through ImageJ software (version 1.53t, NIH, Bethesda, MD, USA). The EdU index was calculated as the ratio of EdU-positive nuclei to total DAPI-stained nuclei in each field.

Invasion Assay

Cell invasive capability was evaluated using Transwell chambers with polycarbonate membranes containing 8-μm pores (#3422, Corning, NY, USA), pre-coated with Matrigel (#356234, Corning, NY, USA) to mimic the extracellular matrix. A suspension of 5×10^4 cells in 200 μL serum-free medium was added to the upper chamber, while the lower chamber was filled with 600 μL medium containing 10% fetal bovine serum as a chemoattractant. After 24 hours of incubation at 37 °C, non-migrated cells on the upper membrane surface were gently removed with a sterile cotton swab. Cells that migrated to the underside of the membrane were fixed with 4% paraformaldehyde (#P1110, Solarbio, Beijing, China) for 15 minutes, stained with 0.1% crystal violet (#C0121, Beyotime, Shanghai, China) for 20 minutes, and rinsed with PBS. Images from five randomly selected fields were captured under a light microscope (Olympus CKX53, Olympus, Tokyo, Japan), and invading cells were quantified using ImageJ software (version 1.53t, NIH, Bethesda, MD, USA).

Migration Assays

A549 and H1299 cells were seeded into 6-well plates and grown to approximately 90% confluency. A straight scratch was created across the cell monolayer using a sterile 200-μL pipette tip to simulate a wound. Detached cells and debris were removed by gentle washing with PBS. The cells were then cultured in serum-free RPMI-1640 medium to minimize proliferation effects.

Images of the scratched area were taken at both 0 and 24 hours after scratching using an inverted phase-contrast microscope (Olympus CKX53, Olympus, Tokyo, Japan). The wound width at each time point was measured using ImageJ software (version 1.53t, NIH, Bethesda, MD, USA), and the migration rate was determined according to the formula: wound closure = (W0 - W24h) / W0.

Mitochondrial Membrane Potential Assay

Mitochondrial membrane potential ($\Delta\Psi m$) was measured using the JC-1 Mitochondrial Membrane Potential Assay Kit (#C2006, Beyotime, Shanghai, China), following the manufacturer's instructions. Briefly, A549 and H1299 cells were seeded into 6-well plates and transfected as described previously. After 48 hours, cells were stained with JC-1 dye at 37 °C for 20 minutes in the dark. Excess dye was removed by washing with JC-1 buffer. Fluorescent signals were captured using an Olympus IX73 fluorescence microscope (Olympus, Tokyo, Japan). A reduction in the red-to-green fluorescence ratio indicated depolarization of the mitochondrial membrane. Fluorescence intensity was quantified using ImageJ software (version 1.53t, NIH, Bethesda, MD, USA).

Assessment of Intracellular Energy Metabolism

Cellular energy metabolism was assessed by measuring adenosine triphosphate (ATP) and nicotinamide adenine dinucleotide/reduced nicotinamide adenine dinucleotide (NAD^+/NADH) levels. ATP levels were determined using the ATP Assay Kit (#ab83355, Abcam, Cambridge, MA, USA). Forty-eight hours post-treatment, A549 and H1299 cells were collected, lysed on ice, and cen-

trifuged at 12,000 ×g for 5 minutes at 4 °C. Equal volumes of supernatant and ATP detection reagent were added to a white 96-well plate. After a 30-minute incubation at room temperature, absorbance was measured at 570 nm using a microplate reader (SpectraMax iD3, Molecular Devices, San Jose, CA, USA). ATP concentrations were calculated based on a standard curve generated from known ATP standards.

For NAD^+/NADH analysis, the NAD^+/NADH Assay Kit (#ab176723, Abcam, Cambridge, MA, USA) was used. Cells underwent lysis and centrifugation under similar conditions to obtain the supernatant. To determine NADH levels, samples were incubated at 60 °C for 30 minutes. Absorbance readings at 450 nm allowed quantification of total NAD and NADH, with NAD^+ levels calculated by subtracting NADH from total NAD.

ROS Detection

ROS levels were measured using a 2',7'-dichlorodihydrofluorescein diacetate (DCFH-DA)-based ROS Detection Kit (#S0033S, Beyotime, Shanghai, China) according to the manufacturer's instructions. A549 and H1299 cells were seeded in 6-well plates and subjected to the specified treatments. After 48 hours, cells were incubated with 10 µM DCFH-DA in serum-free medium at 37 °C for 30 minutes in the dark. Cells were then washed three times with serum-free medium to remove unbound probe. Fluorescence signals were captured using a fluorescence microscope (Olympus IX73, Olympus, Tokyo, Japan) with excitation and emission wavelengths of 488 nm and 525 nm, respectively. Mean fluorescence intensity was quantified using ImageJ software (version 1.53t, NIH, Bethesda, MD, USA) and normalized to the control group (set as 100%) to determine relative ROS levels.

Caspase-3 and Caspase-9 Activity Assay

Caspase-3 (#C1115, Beyotime, Shanghai, China) and Caspase-9 (#C1157, Beyotime, Shanghai, China) activities in A549 and H1299 cells were measured using commercial enzyme-linked immunosorbent assay (ELISA) kits according to the manufacturer's instructions. Forty-eight hours post-treatment, cells were collected, lysed, and centrifuged at 12,000 ×g for 5 minutes at 4 °C. Supernatants were added to antibody-coated 96-well plates, incubated with detection reagents, and absorbance was measured at 405 nm using a microplate reader (SpectraMax iD3, Molecular Devices, USA). Caspase activities were quantified based on standard curves.

NAC Treatment

Pretreatment with the ROS scavenger N-acetylcysteine (NAC; 10 mM, 1h) (#1009005, Sigma-Aldrich, St. Louis, MO, USA) was performed in the A549 cells [12]. After NAC pretreatment, cells were transfected with siAURKA for 24 hours before subsequent analyses.

TUNEL Assay

The detection of apoptotic cells was conducted using the terminal deoxynucleotidyl transferase deoxyuridine triphosphate nick end labeling (TUNEL) BrightRed Apoptosis Detection Kit (#C1089, Beyotime, Shanghai, China), strictly following the manufacturer's instructions. A549 and H1299 cell lines were cultured on sterilized glass coverslips and subsequently subjected to fixation in 4% paraformaldehyde solution for 30 minutes at room temperature. After being rinsed thoroughly with PBS, the cells underwent membrane permeabilization through incubation with 0.3% Triton X-100 for 5 minutes under ice-cold conditions. Following this, a TUNEL working solution—comprising terminal deoxynucleotidyl transferase and a fluorescently tagged deoxyuridine triphosphate (dUTP)—was carefully applied to the cells, which were then incubated at 37 °C for 60 minutes in a dark environment to prevent photobleaching of the fluorescent signal.

Nuclei were counterstained with DAPI (1 µg/mL, #C1002, Beyotime, Shanghai, China) for 10 minutes. TUNEL-positive apoptotic cells (red fluorescence) and total nuclei (blue fluorescence) were visualized and imaged using a fluorescence microscope (Olympus IX73, Olympus, Tokyo, Japan). The apoptotic rate was calculated as the ratio of TUNEL-positive cells to the total number of nuclei in randomly selected fields. Quantitative analysis was performed using ImageJ software (version 1.53t; National Institutes of Health, Bethesda, MD, USA), with the apoptotic index expressed as the TUNEL/DAPI ratio.

The Extraction of RNA Accompanied by Quantitative Real-Time PCR (qRT-PCR)

Total RNA was extracted from A549 and H1299 cells using TRIzol™ reagent (#15596026, Thermo Fisher Scientific, Waltham, MA, USA) following the manufacturer's protocol. Subsequently, 1 µg of purified RNA was reverse-transcribed into cDNA using the PrimeScript™ RT reagent Kit with gDNA Eraser (#RR047A, Takara, Tokyo, Japan) to remove genomic DNA contamination.

Quantitative real-time PCR (qRT-PCR) was then performed using TB Green® Premix Ex Taq™ II (#RR820A, Takara, Tokyo, Japan) on the QuantStudio™ 5 Real-Time PCR System (Applied Biosystems, Foster City, CA, USA). Glyceraldehyde-3-phosphate dehydrogenase (*GAPDH*) served as the endogenous reference gene, and relative mRNA levels were analyzed using the $2^{-\Delta\Delta Ct}$ method. The primers used in this study are listed in Table 2.

Western Blot Analysis

Total cellular proteins were extracted by lysing cells in radioimmunoprecipitation buffer (#P0013B, Beyotime, Shanghai, China) supplemented with protease and phosphatase inhibitor cocktails (#P1050, Beyotime, Shanghai, China) to prevent degradation and dephosphorylation. Protein concentration was measured using a bicinchoninic acid

Table 2. Primer sequences used for qRT-PCR.

Gene	Accession number	Primer (5′→3′)
AURKA	NM_198433	F: GCAACCAGTGTACCTCATCCTG
		R: AAGTCTTCCAAAGCCCACTGCC
GAPDH	NM_001101	F: CACCATTGGCAATGAGCGGTTC
		R: AGGTCTTTGCGGATGTCCACGT

qRT-PCR, quantitative real-time PCR; *AURKA*, Aurora kinase A; *GAPDH*, glyceraldehyde-3-phosphate dehydrogenase.

(BCA) assay kit (#P0010, Beyotime, Shanghai, China). Equal amounts of protein (20 µg) were separated by 12% sodium dodecyl sulfate–polyacrylamide gel electrophoresis and transferred onto polyvinylidene difluoride membranes (#IPVH00010, Millipore, Billerica, MA, USA) for further immunoblotting analysis.

Membranes were blocked in 5% non-fat dry milk in tris-buffered saline with tween 20 for 1 hour at room temperature to reduce non-specific binding, then incubated overnight at 4 °C with primary antibodies against AURKA (#91590, 1:1000), b-cell lymphoma 2 (Bcl-2, #3498, 1:1000), bcl-2-associated X protein (Bax, #5023, 1:1000), and GAPDH (#2118, 1:2000) as a loading control. All antibodies were sourced from Cell Signaling Technology (Danvers, MA, USA).

Following thorough washes with TBST buffer to eliminate unbound primary antibodies, the membranes were incubated for 1 hour at ambient temperature with horseradish peroxidase (HRP)-linked secondary antibodies (#7074, Cell Signaling Technology, Danvers, MA, USA, 1:5000). To visualize the protein signals, an enhanced chemiluminescent (ECL) substrate (#WBKLS0500, Millipore, Billerica, MA, USA) was applied according to the manufacturer's instructions. The emitted chemiluminescent signals were captured using the ChemiDoc™ XRS+ imaging system (Bio-Rad, Hercules, CA, USA). Densitometric analysis of the resulting protein bands was subsequently performed using ImageJ software (version 1.53t, National Institutes of Health, Bethesda, MD, USA).

Statistical Analysis

All experiments were independently repeated at least three times. Data are presented as mean ± standard deviation (SD). Statistical analyses were conducted using GraphPad Prism 9.5 (GraphPad Software Inc., San Diego, CA, USA). Comparisons between two groups were performed using a two-tailed unpaired Student's *t*-test, while differences among multiple groups were assessed by one-way analysis of variance followed by Tukey's multiple comparisons test. A p-value < 0.05 was considered statistically significant.

Results

AURKA Is Significantly Upregulated in LUAD and Correlates With Poor Prognosis

In order to investigate AURKA expression in LUAD, publicly available RNA-seq datasets were initially examined via the GEPIA2 online platform. The results revealed that markedly higher AURKA expression levels in LUAD specimens (n = 483) relative to those in non-tumorous lung tissues (n = 347) ($p < 0.05$, Fig. 1a). Further stratification by pathological stage showed that AURKA expression gradually increased with tumor progression. One-way ANOVA revealed a significant difference in AURKA expression across different LUAD stages ($F = 4.1$, $p = 0.00687$; Fig. 1b).

Survival analysis using the GEPIA2 platform and Kaplan–Meier methodology demonstrated that lung adenocarcinoma patients with high AURKA expression had significantly shorter overall survival compared to those with low AURKA levels (log-rank $p = 0.047$, Fig. 1c). These findings suggest that AURKA may serve as a valuable prognostic biomarker in lung adenocarcinoma.

Consistent with these findings, immunohistochemistry data from the HPA revealed strong AURKA immunoreactivity in LUAD tissue samples, while normal lung tissues showed minimal or no staining (Fig. 1d). These observations were further validated at the cellular level. Immunoblotting analysis demonstrated significantly higher AURKA protein expression in lung adenocarcinoma cell lines—A549, H1299, PC9, and H1975—compared to the non-malignant bronchial epithelial cell line BEAS-2B (Fig. 1e, $p < 0.05$). A similar trend was observed at the mRNA level by qRT-PCR (Fig. 1f, $p < 0.05$). Among the tested cell lines, A549 and H1299 exhibited particularly elevated AURKA expression. Consequently, the two cell lines were selected as representative models for subsequent gene silencing experiments to assess the effects of AURKA loss-of-function.

AURKA Knockdown Suppresses Proliferation, Migration, and Invasion in NSCLC Cells

To investigate how AURKA contributes to the initiation and advancement of NSCLC, small interfering RNAs targeting AURKA were delivered into the lung adenocarcinoma cell lines A549 and H1299 using a transfection-based approach. Results obtained from western blot and RT-qPCR assays consistently demonstrated that siRNA interference led to a substantial suppression of AURKA expression in A549 and H1299 cells, as reflected by notable declines in its transcriptional activity and corresponding protein abundance ($p < 0.05$; Fig. 2a,b,e,f). CCK-8 assay results demonstrated that AURKA knockdown led to a significant reduction in the proliferative capacity and metabolic activity of lung adenocarcinoma cell lines A549 and H1299 ($p < 0.05$; Fig. 2c,g).

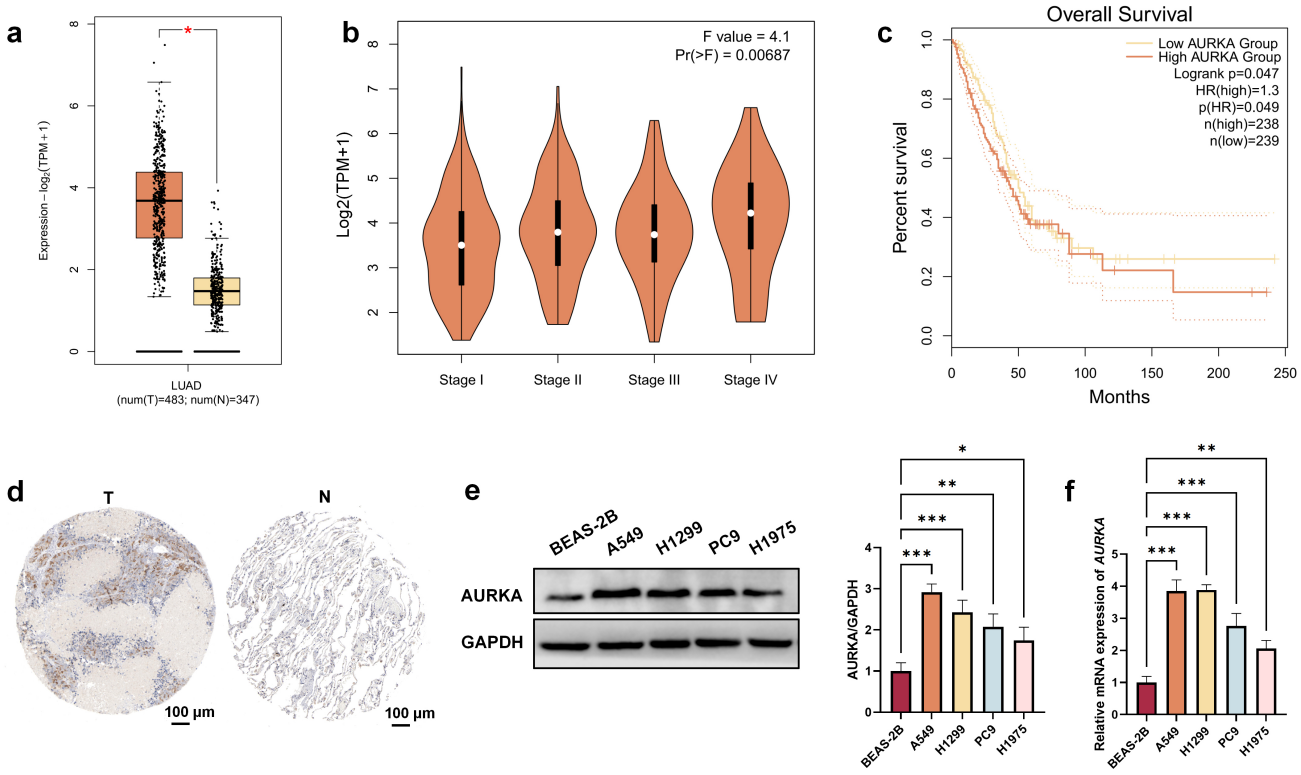

Fig. 1. AURKA expression and related bioinformatic analyses in lung adenocarcinoma (LUAD). (a) AURKA expression in LUAD and normal lung tissues (GEPIA2). (b) AURKA expression across LUAD pathological stages (GEPIA2). (c) Kaplan–Meier overall survival curves based on AURKA expression in LUAD patients (GEPIA2). (d) Immunohistochemical staining of AURKA in normal lung and LUAD tissues (Human Protein Atlas). T: tumor, N: normal. (e) Western blot analysis of AURKA expression in BEAS-2B, A549, H1299, PC9, and H1975 cells. (f) qRT-PCR analysis of AURKA mRNA levels in the same cell lines. Data are shown as mean ± SD, n = 3. *$p < 0.05$, **$p < 0.01$, ***$p < 0.001$.

The colony formation assay demonstrated that reducing AURKA expression markedly impaired the ability of A549 and H1299 lung adenocarcinoma cells to proliferate and form colonies over time ($p < 0.05$; Fig. 2d,h). Additionally, EdU incorporation assays showed a pronounced decline in cellular proliferation following si-AURKA transfection, as compared with the negative control groups in both cell models ($p < 0.05$; Fig. 2i,j).

Transwell invasion and wound healing assays consistently demonstrated that AURKA silencing significantly impaired the invasive ability and motility of both A549 and H1299 lung adenocarcinoma cells ($p < 0.05$; Fig. 2k,l,n,o). Concurrently, western blot analysis showed that AURKA knockdown markedly increased the expression of the epithelial marker E-cadherin while significantly decreasing the mesenchymal marker Vimentin in both cell lines ($p < 0.05$; Fig. 2m,p), suggesting a reversal of epithelial–mesenchymal transition (EMT).

AURKA Knockdown Induces Mitochondrial Dysfunction and Oxidative Stress in NSCLC Cells

To further evaluate how the suppression of AURKA affects mitochondrial integrity and the process of apoptosis, JC-1 staining revealed a significant decrease in mitochondrial membrane potential within A549 and H1299 cells that had undergone transfection with si-AURKA compared to those treated with si-NC (Fig. 3a,b; $p < 0.05$). Measurement of intracellular NAD^+, NADH, and the NAD^+/NADH ratio revealed disrupted mitochondrial redox balance in A549 and H1299 cells following AURKA silencing (Fig. 3c,d; $p < 0.05$). Correspondingly, ATP levels were significantly reduced in si-AURKA groups versus si-NC in both cell lines (Fig. 3e,f; $p < 0.05$).

DCFH-DA fluorescence staining indicated a significant increase in ROS levels within A549 and H1299 cells following transfection with AURKA siRNA, relative to cells treated with the negative control siRNA (Fig. 3g,h; $p < 0.05$). Increased apoptotic activity was detected in A549 and H1299 cells following AURKA silencing, as evidenced by TUNEL assay results (Fig. 3i,j; $p < 0.05$). In A549 and H1299 cells treated with si-AURKA, Bax expression was elevated while Bcl-2 levels were reduced, as determined by western blot (Fig. 3k,m; $p < 0.05$). Furthermore, ELISA results indicated enhanced enzymatic activities of Caspase-3 and Caspase-9 (Fig. 3l,n; $p < 0.05$).

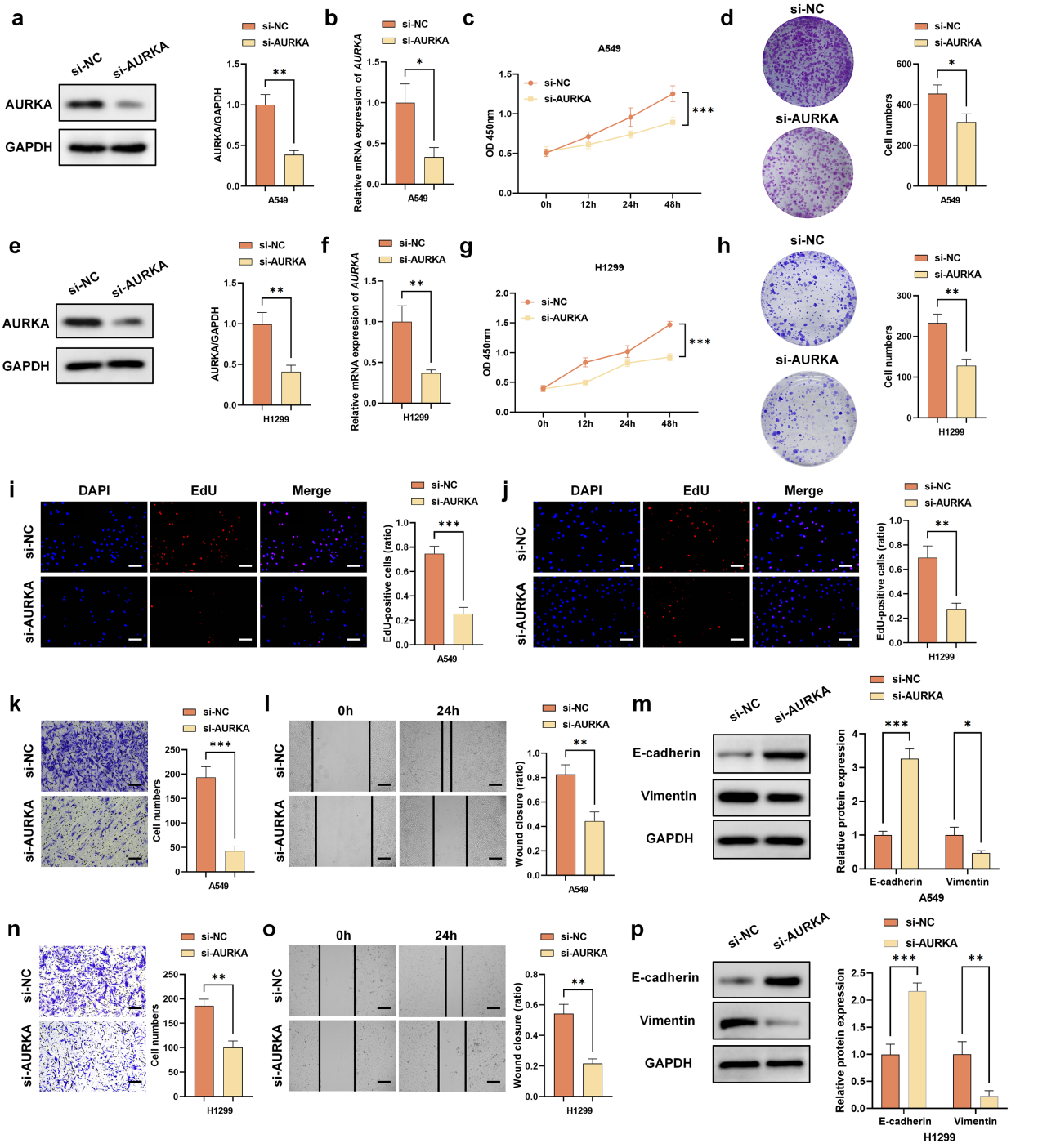

Fig. 2. Functional analysis of AURKA knockdown in non-small cell lung cancer (NSCLC) cells. A549 and H1299 cells were transfected with si-NC or si-AURKA for subsequent assays. (a) Western blot analysis of AURKA protein in A549 cells. (b) qRT-PCR of *AURKA* mRNA in A549 cells. (c) Cell counting kit-8 (CCK-8) assay for A549 cell viability. (d) Colony formation in A549 cells. (e) Western blot analysis of AURKA protein in H1299 cells. (f) qRT-PCR analysis of *AURKA* mRNA in H1299 cells. (g) CCK-8 assay for H1299 cell viability. (h) Colony formation in H1299 cells. (i) 5-ethynyl-2′-deoxyuridine (EdU) assay for proliferation in A549 cells. (j) EdU assay for proliferation in H1299 cells. (k) Transwell invasion assay in A549 cells. (l) Wound healing assay in A549 cells. (m) Western blot analysis of E-cadherin and Vimentin in A549 cells. (n) Transwell invasion assay in H1299 cells. (o) Wound healing assay in H1299 cells. (p) Western blot analysis of E-cadherin and Vimentin in H1299 cells. Scale bars: 50 μm (×200 magnification). Data are shown as mean ± SD, n = 3. *$p < 0.05$, **$p < 0.01$, ***$p < 0.001$.

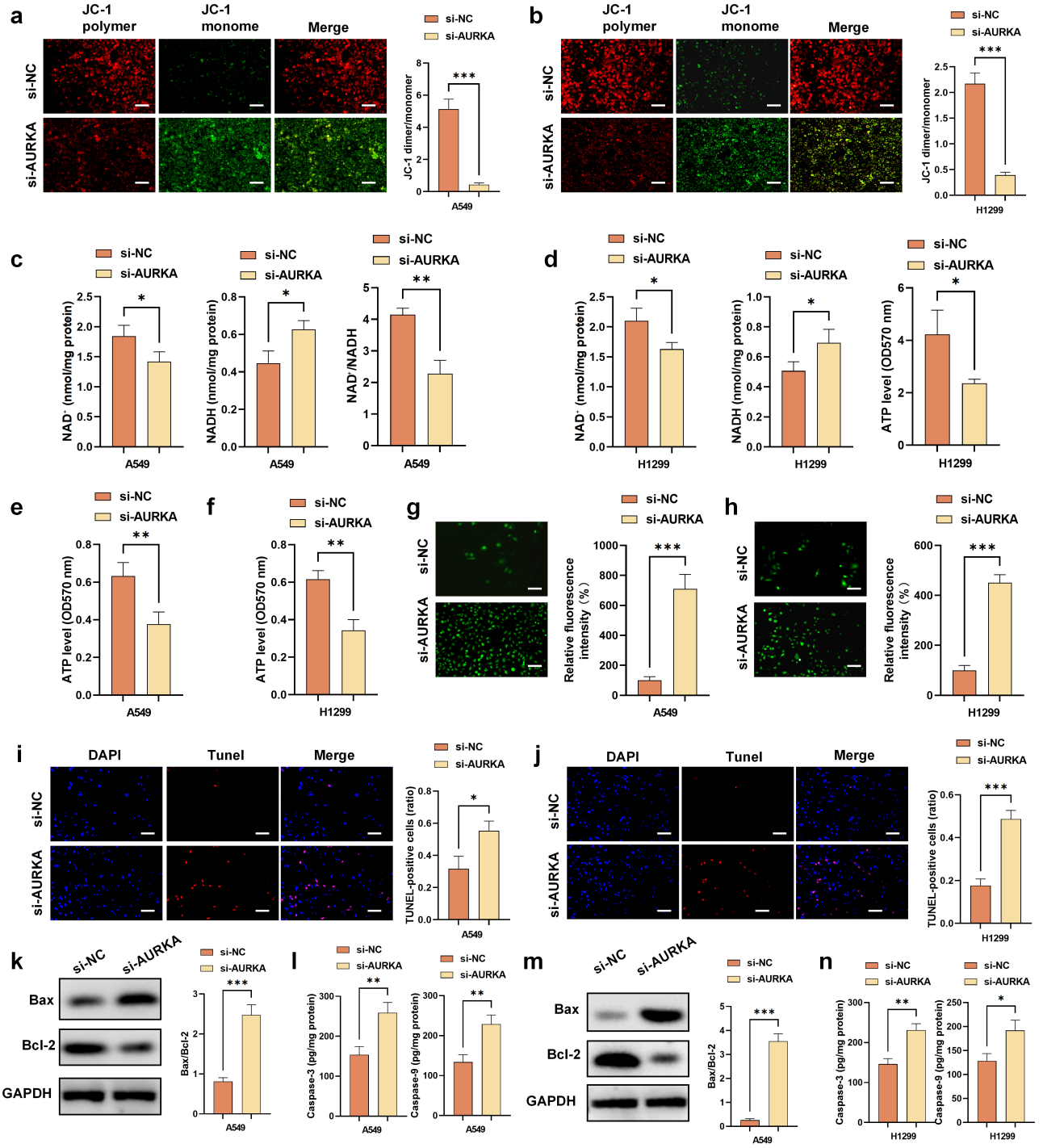

Fig. 3. Effects of AURKA knockdown on mitochondrial function and redox homeostasis in NSCLC cells. A549 and H1299 cells were transfected with si-NC or si-AURKA for subsequent assays. (a,b) JC-1 staining of mitochondrial membrane potential in A549 and H1299 cells. (c,d) nicotinamide adenine dinucleotide (NAD^+), reduced nicotinamide adenine dinucleotide (NADH) levels and their ratio in A549 and H1299 cells. (e,f) adenosine triphosphate (ATP) levels in A549 and H1299 cells. (g,h) 2′,7′-dichlorodihydrofluorescein diacetate (DCFH-DA) staining of reactive oxygen species (ROS) in A549 and H1299 cells. (i,j) terminal deoxynucleotidyl transferase dUTP nick end labeling (TUNEL) assay for apoptosis in A549 and H1299 cells. (k,l) Western blot analysis of b-cell lymphoma 2 (Bcl-2) and bcl-2-associated X protein (Bax) in A549 and H1299 cells. (m,n) enzyme-linked immunosorbent assay (ELISA) measurement of Caspase-3 and Caspase-9 activity in A549 and H1299 cells. Scale bars: 50 µm (×200 magnification). Data are shown as mean ± SD, n = 3. *$p < 0.05$, **$p < 0.01$, ***$p < 0.001$.

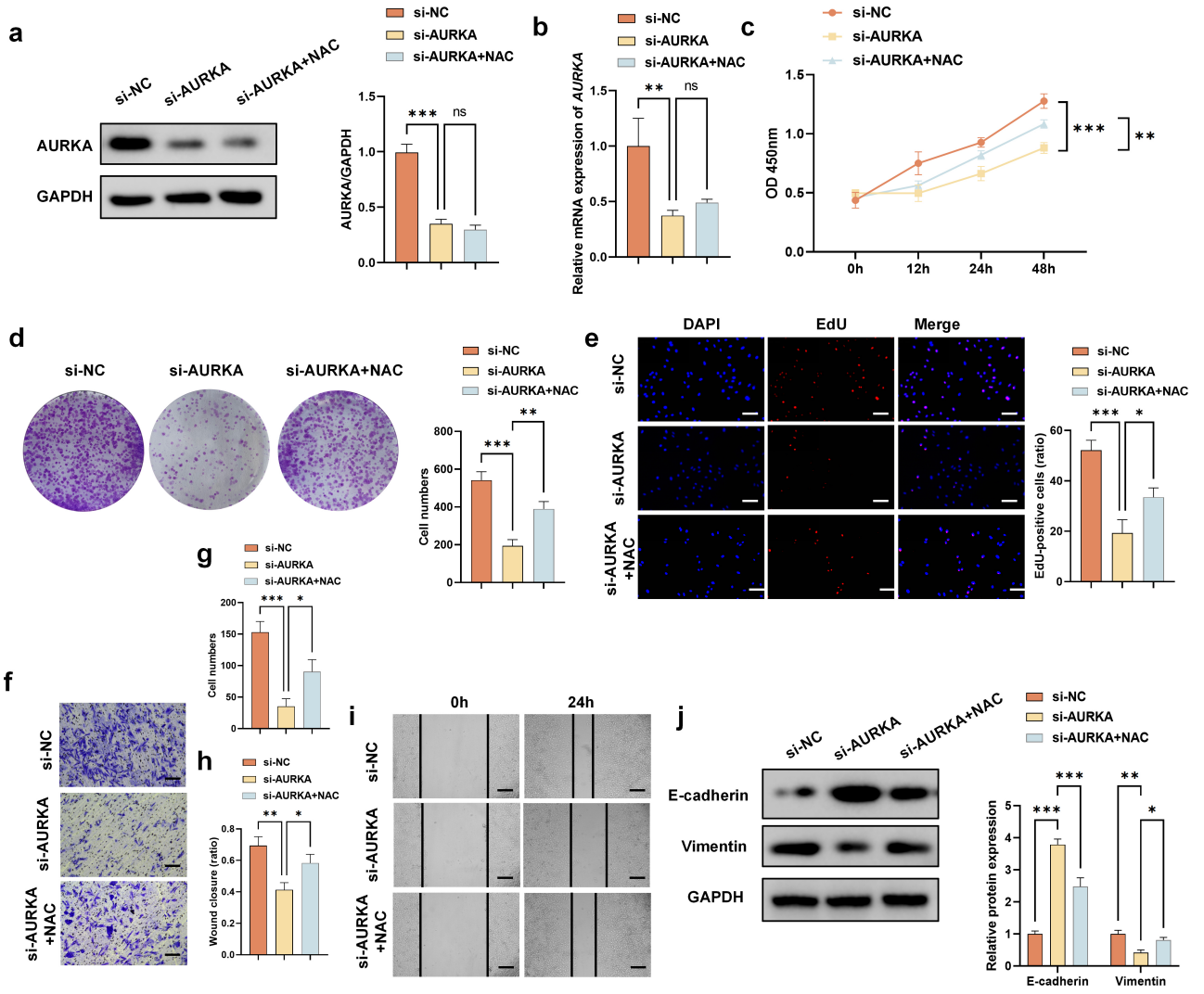

Fig. 4. N-acetylcysteine (NAC) treatment alleviates proliferation, migration, and invasion inhibition caused by AURKA knockdown in A549 cells. A549 cells were transfected with si-NC or si-AURKA and treated with or without NAC (10 mM) for subsequent assays. (a) Western blot analysis of AURKA expression. (b) qRT-PCR analysis of *AURKA* mRNA. (c) CCK-8 assay for viability. (d) Colony formation assay. (e) EdU proliferation assay. (f,g) Transwell invasion assays. (h,i) Wound healing assay. (j) Western blot analysis of E-cadherin and Vimentin. Scale bars: 50 μm (×200 magnification). Data are presented as mean ± SD, n = 3. ns $p > 0.05$, *$p < 0.05$, **$p < 0.01$, ***$p < 0.001$.

These findings imply that silencing AURKA leads to mitochondrial impairment, elevated oxidative stress, and increased apoptotic activity in A549 and H1299 cells.

NAC Administration Effectively Reversed the Impaired Proliferative, Migratory, and Invasive Capabilities of A549 Cells Caused by AURKA Knockdown

To investigate whether oxidative stress contributes to the tumor-suppressive effects induced by AURKA knockdown in A549 and H1299 cells, we selected A549 cells for NAC rescue experiments due to their higher sensitivity to ROS modulation and more pronounced responses in preliminary assays. A549 cells were treated with or without NAC following siRNA transfection. NAC treatment did not significantly affect AURKA expression at either the mRNA or protein level (Fig. 4a,b; $p > 0.05$). However, NAC markedly restored the proliferation of si-AURKA–transfected cells, as demonstrated by increased cell viability, colony formation, and EdU incorporation (Fig. 4c–e; $p < 0.05$). Furthermore, the invasion and migration capabilities suppressed by AURKA knockdown were partially rescued by NAC treatment, as evidenced by Transwell invasion and wound healing assays (Fig. 4f–i; $p < 0.05$). Western blot analysis confirmed that NAC attenuated the si-AURKA–induced upregulation of E-cadherin and downregulation of Vimentin, indicating a partial reversal of EMT-related changes (Fig. 4j; $p < 0.05$).

These findings suggest that ROS accumulation contributes to the impaired proliferative and invasive capacity induced by AURKA silencing in A549 cells.

NAC Alleviates Mitochondrial Dysfunction and Apoptosis Induced by AURKA Knockdown in A549 Cells

To further clarify whether oxidative stress mediates the mitochondrial dysfunction and apoptosis induced by AURKA knockdown, A549 cells were transfected with si-AURKA and subsequently treated with NAC.

JC-1 staining showed that NAC effectively restored mitochondrial membrane potential in si-AURKA-treated cells (Fig. 5a; $p < 0.05$). NAD^+/NADH ratio and intracellular ATP levels, both reduced following AURKA knockdown, were significantly increased upon NAC supplementation (Fig. 5b,c; $p < 0.05$), indicating recovery of mitochondrial metabolic function. DCFH-DA staining revealed that NAC markedly attenuated ROS accumulation induced by AURKA silencing (Fig. 5d; $p < 0.05$).

Consistently, TUNEL assays demonstrated that NAC administration markedly decreased apoptosis in A549 cells following AURKA knockdown (Fig. 5e; $p < 0.05$). Western blot analysis revealed that NAC treatment effectively reversed the Bax upregulation and the associated reduction in Bcl-2 expression caused by AURKA knockdown (Fig. 5f; $p < 0.05$), and ELISA assays confirmed a reduction in Caspase-3 and Caspase-9 activity after NAC treatment (Fig. 5g; $p < 0.05$).

These results suggest that the mitochondrial dysfunction and apoptosis induced by AURKA knockdown are largely mediated by increased ROS levels, and that NAC treatment effectively mitigates these effects.

Discussion

NSCLC—which includes LUAD, squamous cell carcinoma, and large cell carcinoma—is characterized by high heterogeneity and poor prognosis [13]. Growing evidence highlights the oncogenic role of AURKA, a serine/threonine kinase essential for mitotic progression, in the initiation and progression of various cancers [14]. However, the specific functions of AURKA in NSCLC progression, particularly its potential involvement in mitochondrial function and redox homeostasis, remain poorly understood. This study aims to elucidate the biological roles and underlying regulatory mechanisms of AURKA in NSCLC and to investigate whether oxidative stress acts as a critical mediator of AURKA-associated tumor phenotypes.

AURKA is frequently overexpressed in a variety of cancers and is associated with aggressive tumor behavior and poor patient prognosis [15–17]. Consistent with these reports, our bioinformatics analyses and experimental data revealed a significant upregulation of AURKA in LUAD tissues and NSCLC cell lines compared to normal controls. Moreover, elevated AURKA expression correlated with advanced pathological stages and decreased overall survival. Functionally, silencing AURKA resulted in a substantial reduction in proliferation, colony formation, migration, and invasion in A549 and H1299 cells. These findings align with previous studies in breast [18], ovarian [19], and liver [20] cancers, where AURKA knockdown disrupted cell cycle progression and impaired metastatic potential, reinforcing its critical role as an oncogenic driver in NSCLC.

Notably, our mechanistic investigations revealed that AURKA knockdown induces significant mitochondrial dysfunction, as demonstrated by several key indicators. JC-1 staining showed a marked reduction in mitochondrial membrane potential, indicative of compromised mitochondrial integrity and a hallmark of early apoptosis [21]. Concurrently, assessment of the NAD^+/NADH ratio revealed disrupted mitochondrial redox balance, essential for maintaining metabolic homeostasis and efficient oxidative phosphorylation [21,22]. ATP quantification further confirmed that silencing AURKA impairs mitochondrial bioenergetics. These metabolic disturbances coincided with elevated intracellular ROS levels, suggesting increased oxidative stress that can damage cellular components and trigger apoptosis [23]. Although tumor cells typically exhibit heightened ROS levels that support proliferation and survival, AURKA knockdown led to further ROS accumulation accompanied by mitochondrial dysfunction and apoptosis. These findings imply that AURKA deficiency–induced apoptosis may be linked to ROS accumulation, although further research is necessary to clarify AURKA's precise regulatory role in ROS homeostasis [24]. Supporting this, pro-apoptotic markers were upregulated: Bax expression increased significantly, while the anti-apoptotic protein Bcl-2 decreased, alongside enhanced activities of Caspase-3 and Caspase-9 [25]. Similar mitochondrial and apoptotic effects have been reported in colon [26] and ovarian [27] cancer models following AURKA inhibition, underscoring AURKA's critical role in maintaining mitochondrial integrity and redox homeostasis. To determine whether oxidative stress mediates these effects, rescue experiments using the antioxidant NAC were performed in A549 cells. NAC treatment effectively restored cell viability, migration, and invasion, while reversing mitochondrial dysfunction and suppressing ROS accumulation. Collectively, these results suggest that ROS acts as a key mediator linking AURKA deficiency to mitochondrial impairment and apoptosis signaling pathways.

Despite the robust findings, several limitations should be acknowledged. First, NAC rescue assays were conducted solely in A549 cells, and whether similar effects occur in other NSCLC models remains to be confirmed. Second, although ROS was identified as a key mediator, the upstream molecular mechanisms by which AURKA regulates redox homeostasis require further investigation. Additionally, potential interactions between AURKA

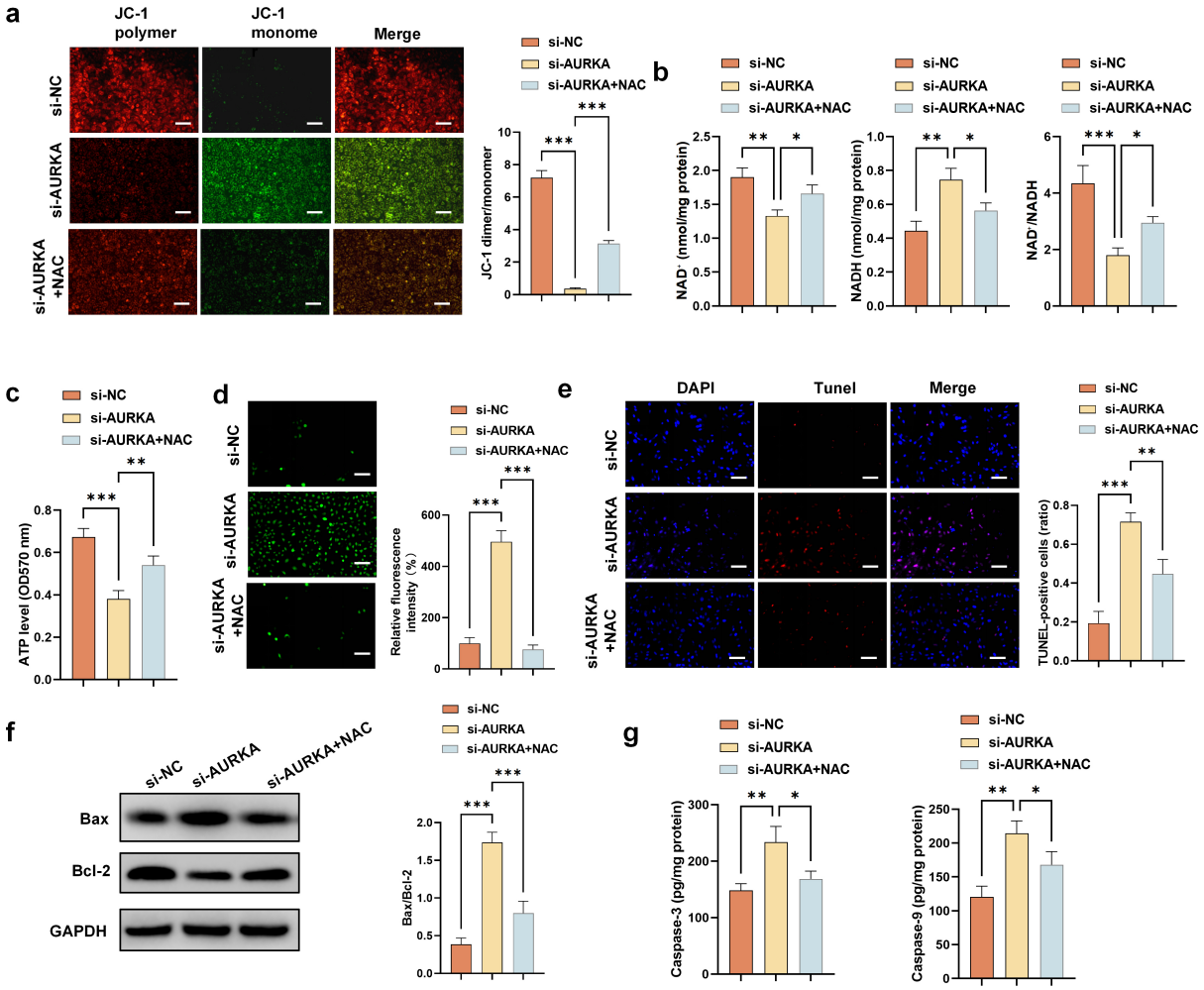

Fig. 5. Effects of NAC treatment on mitochondrial function, redox balance, and apoptosis in AURKA-silenced A549 cells. A549 cells were transfected with si-NC or si-AURKA and treated with or without NAC (10 mM). (a) JC-1 staining of mitochondrial membrane potential. (b) NAD^+, NADH levels and their ratio. (c) ATP levels. (d) DCFH-DA staining for ROS. (e) TUNEL assay for apoptosis. (f) Western blot analysis of Bax and Bcl-2. (g) ELISA measurement of Caspase-3 and Caspase-9 activity. Scale bars: 50 μm (×200 magnification). Data are presented as mean ± SD, n = 3. *$p < 0.05$, **$p < 0.01$, ***$p < 0.001$.

and mitochondrial quality control processes—such as mitophagy or mitochondrial fission/fusion dynamics—were not explored and may offer further mechanistic insights. Lastly, while siRNA-mediated knockdown demonstrated AURKA's functional role, pharmacological inhibition using specific AURKA inhibitors was not assessed. Future studies incorporating such inhibitors would strengthen the translational relevance of these findings.

Conclusion

In conclusion, our study demonstrates that AURKA facilitates NSCLC progression by preserving mitochondrial integrity and suppressing oxidative stress. Targeting the AURKA–ROS–mitochondrial axis may offer a novel therapeutic approach to disrupt tumor growth and improve clinical outcomes in NSCLC patients.

Availability of Data and Materials

The datasets used and/or analyzed during the current study are available from the corresponding author on reasonable request.

Author Contributions

XW and LX conceptualized and designed the study. XW performed the majority of the experiments and data analysis. XW and LX contributed to data acquisition and interpretation. LX provided guidance and supervision throughout the research process. XW drafted the manuscript, and both authors revised it critically for important intellectual content. Both authors contributed to editorial changes in the manuscript. Both authors read and approved the final manuscript. Both authors have participated sufficiently in the work and agreed to be accountable for all aspects of the work.

Ethics Approval and Consent to Participate

Not applicable.

Acknowledgment

Not applicable.

Funding

This research was funded by the Science and Technology Program of Wenzhou (No. S20240012).

Conflict of Interest

The authors declare no conflict of interest.

References

[1] Sung H, Ferlay J, Siegel RL, Laversanne M, Soerjomataram I, Jemal A, *et al*. Global Cancer Statistics 2020: GLOBOCAN Estimates of Incidence and Mortality Worldwide for 36 Cancers in 185 Countries. CA: a Cancer Journal for Clinicians. 2021; 71: 209–249. https://doi.org/10.3322/caac.21660.

[2] Shen Y, Chen JQ, Li XP. Differences between lung adenocarcinoma and lung squamous cell carcinoma: Driver genes, therapeutic targets, and clinical efficacy. Genes & Diseases. 2024; 12: 101374. https://doi.org/10.1016/j.gendis.2024.101374.

[3] Wang W, Liu H, Li G. What's the difference between lung adenocarcinoma and lung squamous cell carcinoma? Evidence from a retrospective analysis in a cohort of Chinese patients. Frontiers in Endocrinology. 2022; 13: 947443. https://doi.org/10.3389/fendo.2022.947443.

[4] Gálffy G, Morócz É, Korompay R, Hécz R, Bujdosó R, Puskás R, *et al*. Targeted therapeutic options in early and metastatic NSCLC-overview. Pathology and Oncology Research. 2024; 30: 1611715. https://doi.org/10.3389/pore.2024.1611715.

[5] Zheng D, Li J, Yan H, Zhang G, Li W, Chu E, *et al*. Emerging roles of Aurora-A kinase in cancer therapy resistance. Acta Pharmaceutica Sinica. B. 2023; 13: 2826–2843. https://doi.org/10.1016/j.apsb.2023.03.013.

[6] Chen M, Zhu H, Li J, Luo D, Zhang J, Liu W, *et al*. Research progress on the relationship between AURKA and tumorigenesis: the neglected nuclear function of AURKA. Annals of Medicine. 2024; 56: 2282184. https://doi.org/10.1080/07853890.2023.2282184.

[7] Sun C, Qu Z, Liu W, Qiu Z, Lü Y, Sun Z. The Synergistic Anti-colon Cancer Effect of Aurora A Inhibitors and AKT Inhibitors Through PI3K/AKT Pathway. Anti-cancer Agents in Medicinal Chemistry. 2023; 23: 87–93. https://doi.org/10.2174/1871520622666220422133537.

[8] Liu F, Zhang Y, Dong Y, Ning P, Zhang Y, Sun H, *et al*. Knockdown of AURKA sensitizes the efficacy of radiation in human colorectal cancer. Life Sciences. 2021; 271: 119148. https://doi.org/10.1016/j.lfs.2021.119148.

[9] Wang J, Hu T, Wang Q, Chen R, Xie Y, Chang H, *et al*. Repression of the AURKA-CXCL5 axis induces autophagic cell death and promotes radiosensitivity in non-small-cell lung cancer. Cancer Letters. 2021; 509: 89–104. https://doi.org/10.1016/j.canlet.2021.03.028.

[10] Feng F, He S, Li X, He J, Luo L. Mitochondria-mediated Ferroptosis in Diseases Therapy: From Molecular Mechanisms to Implications. Aging and Disease. 2024; 15: 714–738. https://doi.org/10.14336/AD.2023.0717.

[11] Sharma RK, Chafik A, Bertolin G. Aurora kinase A/AURKA functionally interacts with the mitochondrial ATP synthase to regulate energy metabolism and cell death. Cell Death Discovery. 2023; 9: 203. https://doi.org/10.1038/s41420-023-01501-2.

[12] Zhang D, Yuan R, Pan J, Fan Q, Sun K, Xu Z, *et al*. Dihydrotanshinone Triggers Porimin-Dependent Oncosis by ROS-Mediated Mitochondrial Dysfunction in Non-Small-Cell Lung Cancer. International Journal of Molecular Sciences. 2023; 24: 11953. https://doi.org/10.3390/ijms241511953.

[13] Huang D, Wang J, Chen L, Jiang W, Inuzuka H, Simon DK, *et al*. Molecular Subtypes and Targeted Therapeutic Strategies in Small Cell Lung Cancer: Advances, Challenges, and Future Perspectives. Molecules (Basel, Switzerland). 2025; 30: 1731. https://doi.org/10.3390/molecules30081731.

[14] Du R, Huang C, Liu K, Li X, Dong Z. Targeting AURKA in Cancer: molecular mechanisms and opportunities for Cancer therapy. Molecular Cancer. 2021; 20: 15. https://doi.org/10.1186/s12943-020-01305-3.

[15] Wen J, Wang X, Yang G, Zheng J. AURKA promotes renal cell carcinoma progression via regulation of CCNB1 transcription. Heliyon. 2024; 10: e27959. https://doi.org/10.1016/j.heliyon.2024.e27959.

[16] Jiang J, Guo Z, Xu J, Sun T, Zheng X. Identification of Aurora Kinase A as a Biomarker for Prognosis in Obesity Patients with Early Breast Cancer. OncoTargets and Therapy. 2020; 13: 4971–4985. https://doi.org/10.2147/OTT.S250619.

[17] Ye Y, Xu L, Zhang L, Zhao P, Cai W, Fu G, *et al*. Meningioma achieves malignancy and erastin-induced ferroptosis resistance through FOXM1-AURKA-NRF2 axis. Redox Biology. 2024; 72: 103137. https://doi.org/10.1016/j.redox.2024.103137.

[18] Wang F, Zhang H, Wang H, Qiu T, He B, Yang Q. Combination of AURKA inhibitor and HSP90 inhibitor to treat breast cancer with AURKA overexpression and TP53 mutations. Medical Oncology (Northwood, London, England). 2022; 39: 180. https://doi.org/10.1007/s12032-022-01777-x.

[19] Sun Y, Zhang S, Zhang X, Li G, Sun F, Wang M, *et al*. AURKA Enhances the Glycolysis and Development of Ovarian Endometriosis Through ERβ. Endocrinology. 2024; 165: bqae018. https://doi.org/10.1210/endocr/bqae018.

[20] Liu Z, Wu B, Liu X, Wu X, Du J, Xia G, *et al*. CD73/NT5E-mediated ubiquitination of AURKA regulates alcohol-related liver fibrosis via modulating hepatic stellate cell senescence. International Journal of Biological Sciences. 2023; 19: 950–966. https://doi.org/10.7150/ijbs.80461.

[21] Gong Y, Luo S, Fan P, Zhu H, Li Y, Huang W. Growth hormone activates PI3K/Akt signaling and inhibits ROS accumulation and apoptosis in granulosa cells of patients with polycystic ovary syndrome. Reproductive Biology and Endocrinology: RB&E. 2020; 18: 121. https://doi.org/10.1186/s12958-020-00677-x.

[22] Lu MJ, Busquets J, Impedovo V, Wilson CN, Chan HR, Chang YT, *et al*. SLC25A51 decouples the mitochondrial NAD^+/NADH ratio to control proliferation of AML cells. Cell Metabolism. 2024; 36: 808–821.e6. https://doi.org/10.1016/j.cmet.2024.01.013.

[23] Palma FR, Gantner BN, Sakiyama MJ, Kayzuka C, Shukla S, Lacchini R, *et al*. ROS production by mitochondria: function or dysfunction? Oncogene. 2024; 43: 295–303. https://doi.org/10.1038/s41388-023-02907-z.

[24] Wang X, Zhou Y, Ning L, Chen J, Chen H, Li X. Knockdown of ANXA10 induces ferroptosis by inhibiting autophagy-mediated TFRC degradation in colorectal cancer. Cell Death & Disease. 2023; 14: 588. https://doi.org/10.1038/s41419-023-06114-2.

[25] Hu Y, Wen Q, Cai Y, Liu Y, Ma W, Li Q, *et al*. Alantolactone induces concurrent apoptosis and GSDME-dependent py-

roptosis of anaplastic thyroid cancer through ROS mitochondria-dependent caspase pathway. Phytomedicine: International Journal of Phytotherapy and Phytopharmacology. 2023; 108: 154528. https://doi.org/10.1016/j.phymed.2022.154528.

[26] Liu X, Zhang Y, Wu S, Xu M, Shen Y, Yu M, *et al*. Palmatine induces G2/M phase arrest and mitochondrial-associated pathway apoptosis in colon cancer cells by targeting AURKA. Biochemical Pharmacology. 2020; 175: 113933. https://doi.org/10.1016/j.bcp.2020.113933.

[27] Sachdeva A, Roy A, Gupta MK, Mandal S. Pharmacological inhibition of protein kinase D2/Aurora kinase A signalling axis suppresses G2/M cell cycle progression and proliferation of epithelial ovarian cancer cells. Pathology, Research and Practice. 2024; 260: 155390. https://doi.org/10.1016/j.prp.2024.155390.